JOURNAL OF OPTOELECTRONICS AND ADVANCED MATERIALS Vol. 11, No. 3, March 2009, p. 331 - 337

Optical characterization of hydrothermally grown SnO_2 nanocrystals

A. SHARMA, D. PRAKASH[a], K. D.VERMA[*]
Material Science Research Laboratory, Department of Physics, S.V.College, Aligarh (U.P.) India
[a]School of Computer Science & Engineering, SMVD University, Kakryal (J & K) India

A simple hydrothermal process is proposed for the synthesis of SnO_2 nanoparticles in which ammonium hydroxide is used as the mineralizer. The crystal structure and size of the SnO_2 nanoparticles were determined by X-ray diffraction. Optical properties of so formed nanoparticles were explored by UV-Vis absorption, Photoluminescence, and Raman studies. Experimental results indicate that the as-prepared SnO_2 may have large amount of defects and local lattice disorders at the interface and surface. The visible emission from nanocrystalline SnO_2 is interpreted in terms of the size of the crystals and the presence of the defects in the material. The appearance of new Raman peak marks an additional characteristic of space symmetry due to the agglomeration of grains in nanocrystalline tin oxide.

(Received October 27, 2008; accepted March 19, 2009)

Keywords: SnO_2, X-Ray Diffraction, Hydrothermal process, Nanocrystals

1. Introduction

Low dimensional inorganic nanostructured materials have evoked much interest owing to their possible applications in technological fields. The preparation of nanosized crystallites with different morphologies provides an opportunity to explore the possible changes in their physical and chemical features with size and shape. Due to high surface to volume ratio, the surface atoms play an important role in the properties of nanomaterials, which usually have fewer adjacent coordinate atoms and can be treated as defects as compared with the bulk atoms. These defects induce additional electronic states in the band gap, which can mix with the intrinsic states to a substantial extent, which may also influence the spacing of the energy levels and the optical properties of the nanomaterials. Recently, there has been growing interest in the properties of wide band gap oxide nanocrystalline materials such as tin oxide. Tin oxide (SnO_2) is an important metal oxide, n-type wide band gap semiconductor. Due to its outstanding electrical, optical and electrochemical properties, SnO_2 offers wide range of applications in solar cells, catalytic support materials, transparent electrodes and gas sensors [1-7].Though miscellaneous low dimensional nanostructured materials such as nanobelts, nanoribbons, nanowires, nanotubes, and nanoparticles [7-11] have been synthesized by various methods such as, sol-gel method [5-6], thermal evaporation tin oxide powders [9-10], Vapor- Liquid-Solid (VLS) technique [11], Laser ablation [12], chemical vapor deposition (CVD) [13] and spray-pyrolysis [14], etc. However, there is still a great challenge to synthesize single phase nanocrystalline materials by wet chemical methods.

In the past few years, the interface and surface microstructure of nanomaterials have been extensively and intensively investigated. Diversified types of interface-structure models have also been proposed for nanostructural materials [15-16], such as gas like model and order & extended order model. It is common that the peculiar properties of nanomaterials are explained in terms of the interface and surface structures, while the effects from the microstructure of the grains are neglected. In fact, for different preparation methods, the microstructure of nanomaterials can be nanocrystalline, nanoamorphous grain, or nanocluster agglomerations with some crystalline features. Since the grains are the basic component of nanomaterials, changes in their microstructure should inevitable change the physical and chemical properties. Therefore, study of microstructure of grains can help us reveal the general structure of nanomaterials and explain the corresponding experimental results. Several studies have reported the optical properties of tin oxide nanostructures but origin of photoluminescence (PL) emission, optical absorption and Raman Scattering from the low dimensional tin oxide is still not very clear and satisfactory. E.J.H. Lee et al., [17] reported the PL emission is related to free exciton decay process, but in some other studies the positions of emission maxima were lower than the respective band gap of the SnO_2 nanomaterials, these emissions were assigned due to the different luminescent centers such as various defects and dangling bonds in the nanocrystals [18-19]. The Raman techniques can reveal local structural information of amorphous and poorly crystallized materials; usually the disorder induces spectral changes. Tin oxide gives rise to well defined Raman spectra [20-21], and dynamics of rutile tin oxide also has been extensively studied [22-23]. When the SnO_2 grain size is small, the Raman spectrum is modified, at least partially [19, 24]. However, these reports cannot adequately explain the origin of the abnormal Raman spectra. We have synthesized tin oxide nanocrystals using simple hydrothermal process. The trick in the hydrothermal process presented here is the application of ammonium hydroxide, which coordinate with Sn ions to form a complex cluster. In this article we have attempted to present the physical properties of the nanocrystals, namely the optical absorbance, photoluminescence and Raman scattering and to discuss these phenomena in the light of the size of crystals and the presence of the defects in the material.

2. Experimental details

All regents used were of analytical grade without

further purification. First $SnCl_4$ and ammonium hydroxide were taken in 2:1 ratio respectively and then added in to 150ml of deionized water with stirring. Ammonium hydroxide immediately reacted with $SnCl_4$ in the solution to form a slurry-like white precipitate of the hybrid complex between NH_4OH and $SnCl_4$. After 10 minute of stirring and adding NH_4OH drop by drop up to label the pH value of the solution (pH = 7). The solution was transferred in to a Borosil flask of capacity of 200ml and then sealed. The flask was maintained at 200 ^{0}C for 12 hours and cooled naturally to room temperature. The product was centrifuged, filtered out and rinsed with alcohol and deionized water several times, and then dried at 80 ^{0}C for 1 hour in air. The X- ray diffraction (XRD) measurements of the as grown material were carried out using a Bruker D8 advanced diffractometer for determining the crystallinity and orientation of the SnO_2 crystallites using the CuKα radiation having a wave length of 1.540Å. The scanning speed was 1^0/min, and the scanning range was from 20^0 to 80^0. Optical absorption spectra were recorded with the conventional two beam method using UV-VIS spectrometer (Hitachi UV- 3300). The photoluminescence (PL) studies were carried out using Mechelle 900 spectrograph under a 325 nm excitation of He-Cd laser. The Raman scattering measurements were obtained by using invia Raman microscope. Excitation was provided by an argon-ion laser at a wavelength of 514nm and a low incident power to avoid thermal effects.

3. Results and discussion

3.1. Synthesis

In preparation of SnO_2 nanoparticles the mineralizer (ammonium hydroxide) was chosen in such a way that it was basic in nature. The role of the pH value is crucial in determining the size of the nanoparticles [25].The possible chemical reaction to form tin oxide powders can be written as follow:

$$(SnCl_4)_m + (NH_4OH)_n \rightarrow (SnCl_4)_m.(NH_4OH)_n \quad \text{(i)}$$

$$(SnCl_4)_m.(NH_4OH)_n \rightarrow mSn^{+4} + nNH_4OH + 4mCl^- \quad \text{(ii)}$$

$$Sn^{+4} + 4NH_4OH \rightarrow SnO_2\downarrow + 2H_2O + 4NH_4^+ \quad \text{(iii)}$$

Reaction (i) represent the formation of the complex clusters of the tin chlorite and ammonium hydroxide. In reaction (ii) the complex clusters of tin chloride and ammonium hydroxide underwent dissociation when the solution was heated to 200 ^{0}C during the hydrothermal stage. Reaction (iii) represents the formation of SnO_2 nanoparticles via the reaction between Sn^{+4} and OH^- ions formed in the reaction (ii). Furthermore, we believe that the dissociation of the complex reaction (ii) and the formation of the SnO_2 nanoparticles occurred at the local regions of the $(SnCl_4)$m.(NH_4OH)n complex clusters. Therefore during the hydrothermal stage, SnO_2 nanoparticles successfully synthesized without the addition of any surfactant or complexing agent.

3.2. X-ray diffraction measurements

Crystal structure and phase of the product were determined from XRD patterns. XRD spectra of the product are presented in the Fig. 1. The diffraction peaks in this figure are indexed to represent the rutile phase of the SnO_2 matched with JCPDS PDF No. 41-1445, belonging to the space group of $P4_2$ /mnm (a = 4.7382Å and c = 3.1871Å). No peak due to the metallic tin or any other Sn based oxide or hydroxide were observed, indicating the high purity of the final product. The average grain size of the product was about to 34 nm, determined from XRD peaks by using Scherrer formula; $D = K\lambda/\beta\cos\theta$, where K is the Scherrer constant (K= 0.9), λ is the wave length of the incident x- rays, β is the full width at half maximum of the XRD peaks expressed in radian. It is known for tetragonal structure, the lattice parameters can be calculated by:

$$d_{hkl} = \frac{1}{\sqrt{\frac{h^2+k^2}{a^2} + \frac{l^2}{c^2}}} \quad (1)$$

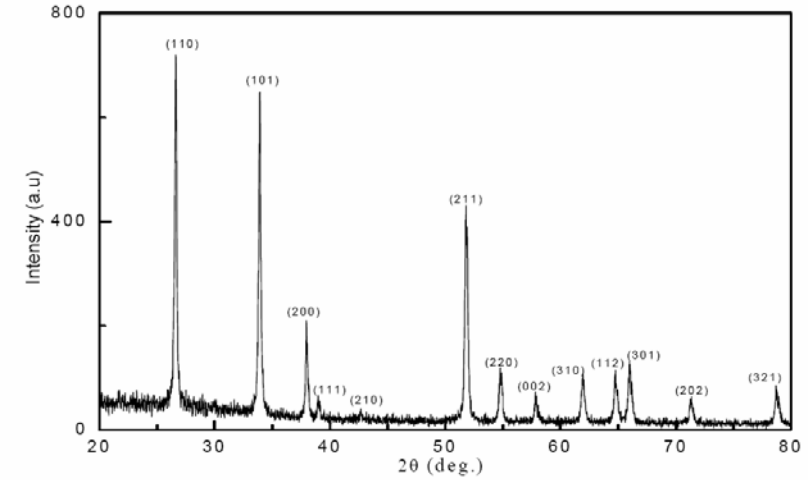

Fig. 1. X-ray diffraction pattern of as-synthesized SnO_2 nanoparticles.

Where h, k, l are all integers, (hkl) is the lattice plane index, a and c are lattice constants. For a real crystal, the calculated values of a and c are the same based on different crystal planes. However, the presence of vacant lattice sites and local lattice disorder may lead to obvious reduction in intensities (or even the disappearance) of XRD peaks of some lattice planes. In this study we observed that the peaks at 62.59^0, 69.23^0 and 74.45^0 corresponding to planes (221), (311) and (212) are absent as compared to standard JCPDS PDF No. 41-1445 and the detailed study of SnO_2 by x-ray diffraction by G.Mc.Carthy et al [26]. Therefore, these results may imply destroyed periodicities in some crystal planes and a significant distortion of the rutile lattice. We have calculated interplaner spacing (d_{hkl}), lattice parameters (a and c) and the difference in the lattice parameters (Δa and Δc) by using the equation (1), as shown in the table (I). From the Table 1, we can see that there is small increase in c and little a decrease in a for the as prepared SnO_2 nanoparticles synthesized by hydrothermal process. This implies that the as prepared SnO_2 may exhibit some local lattice disorder, oxygen vacancies and/or vacancies clusters, which lead to change in the lattice parameters.

*Table 1. Relation of interplaner spacing (d_{hkl}), lattice parameters, and change in the lattice parameters for different samples.**

Index (hkl)	Ref. 26 $d_{(hkl)}$Å	As- prepared $d_{(hkl)}$Å	Lattice parameters and change in lattice parameters for different samples		
			Lattice parameters	(Ref. 26) (Å)	As-prepared(Å)
101	2.6427	2.6433	a_{200}	4.7380	4.7410
200	2.369	2.3705	Δ a	-0.0047	-0.0067
111	2.3094	2.3104	$c_{101\text{-}110}$	3.1856	3.1862
110	3.347	3.3477	a_{110}	4.7333	4.7343
210	2.1189	2.1186	$c_{101\text{-}200}$	3.1839	3.1842
211	1.7641	1.7648	Δ c	0.0017	0.0020
220	1.6750	1.6757			
002	1.5934	1.5946			
310	1.4984	1.4980			
221	1.4829				
112	1.4392	1.4312			
301	1.4155	1.4157			

*Where $\mathbf{a}_{110}$ and $\mathbf{a}_{200}$ are calculated with XRD peaks (110) and (200) respectively; $c_{101\text{-}110}$ and $\mathbf{c}_{101\text{-}200}$ are calculated with peaks (101), (110) and (200) respectively; $\Delta\mathbf{a}$ and $\Delta\mathbf{c}$ are the difference of $\mathbf{a}_{110}$, $\mathbf{a}_{200}$ and $\mathbf{c}_{101\text{-}200}$, respectively

3.3. Optical absorbance studies

UV-visible spectroscopy is an important tool for optical characterization of materials. It provides useful information about the optical band gap of the semiconductors. Fig. 2 shows the optical absorbance spectra of the SnO_2 nanocrystals with photon wavelength in the range of 200-600 nm. As the size of the crystals decreases, the higher surface to volume ratio incorporates various surface related defects in the crystal. This causes a broadening of the absorption spectra at the absorption edge. The optical band gap of the nanocrystalline materials depends on the particle radius due to the quantum confinement effect. The effective mass model is commonly used to study the size dependence of optical properties of the nanocrystals. In this approach the exciton is treated analogously to a hydrogen atom, but is limited by spatial confinement. Therefore the energy of the system is obtained by solving the proper Schrödinger equation. In this manner two regimes are defined according to the coupling of motion of the electron and hole in the exciton: weak and strong confinements. In the former the particle size is larger than exciton Bohr radius (a_B) and the electron and the hole are treated as correlated pair.

The blue shift of the band gap energy is described as;

$$E_g^{eff} = E_g^{bulk} + \frac{\hbar^2\pi^2}{2\mu R^2} \quad (2)$$

In the latter, the nanoparticle radius is below a_B, the electron and hole motion is not correlated and the shift in the band gap energy is given as;

$$E_g^{eff} = E_g^{bulk} + \frac{\hbar^2\pi^2}{2\mu R^2} + \frac{1.8e^2}{\varepsilon R} \quad (3)$$

Where the E_g^{eff} is the band gap of the nanocrystalline material, E_g^{bulk} is the band gap of the material in the bulk form, μ is the effective reduce mass

$(\frac{1}{\mu} = \frac{1}{m_e^*} + \frac{1}{m_h^*}$, where m_e^* and m_h^* are the electron and hole effective masses, respectively) and ε is static dielectric constant of the material. The first term in equation (3) represents the particle- in-a-box quantum localization energy and had simple $1/R^2$ dependence, where R is the particle radius; the second term represents the Coulomb energy with 1/R dependence. Tin oxide has bulk band gap energy (E_g^{bulk}) of 3.6eV and static dielectric constant ε of approximately 14, since $m_e^* << m_h^*$, so the effective reduced mass μ may be replaced by electron effective mass $(m_e^* = 0.275 m_0)$. Therefore the calculated electron Bohr radius a_B is approximately 2.7 nm. The well defined optical band gap of the nanocrystals would have rendered a sharp fall in the transmission spectra at the absorption edge, but we found a broadening associated with absorption edge in the optical absorbance spectra which can obey the carrier-impurity interaction, carrier-phonon interaction and structural disorders. From the optical absorption spectra the band gap of SnO_2 nanocrystals is determined using the Tauc's procedure of plotting $(\alpha h\upsilon)^2$ vs. $h\upsilon$ and extrapolating the linear portion of absorption edge to the energy axis (inset Fig. 2). The band gap of as prepared product was found to be 3.70eV. The increasing in the band gap of the product is attributed to the small crystallites size of the as prepared SnO_2.

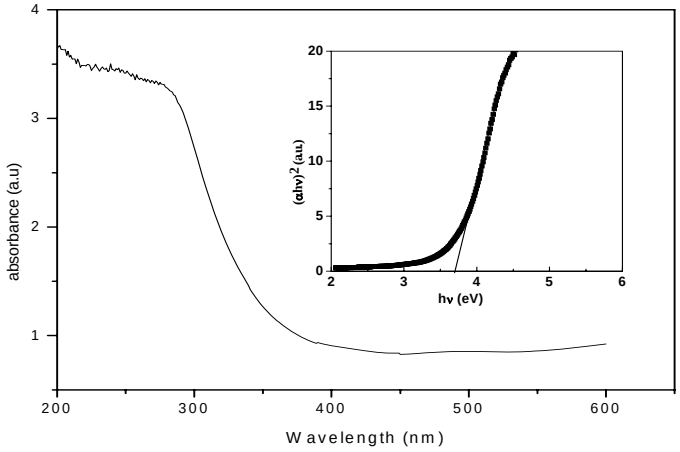

Fig. 2. Optical absorbance spectra of SnO_2 nanoparticles. Inset shows the Tauc plot for the band gap determination.

3.4. Photoluminescence studies

Nanocrystalline SnO_2 displays different PL emission as mentioned in the literature: an UV near band edge emission around 300-350nm [17], and visible emission around 590-620nm [18-19]. Band-edge emission is sharp and strong while other emissions are week and broad. Fig. 3 shows the room temperature photoluminescence spectra of the as synthesized SnO_2 nonocrystals. Since the position of the emission maxima is lower than the respective band gap of the SnO_2 nanocrystals, the emission can not be assigned to the direct recombination of a conduction electron in the Sn 4p band and a hole in the O 2p valence band. So, the PL emission as shown in the figure 3, may be attributed to the different luminescent centers such as various defects and tin interstitials in the nanocrystals. In noncrystalline oxides, oxygen vacancies are known to be most common defect and usually act as the radiative center in the luminescence process. Most commonly the oxygen vacancies are present in the three different charge states in the oxides: V_O, V_O^+ and V_O^{++}. As V_O is very shallow donor, it is expected that most oxygen vacancies will be in their paramagnetic V_O^+ state under the flat band condition, as reported by Soumen Das et.al. [19]. In addition, the visible emission in our PL spectra around 604nm can be assumed to be due to the formation of V_O^{++} luminescent centers. The recombination of surface trapped hole with an electron in deep trap (V_O^+) to form a V_O^{++} centers gives rise to visible emission when a conduction band electron recombines with the V_O^{++} center.

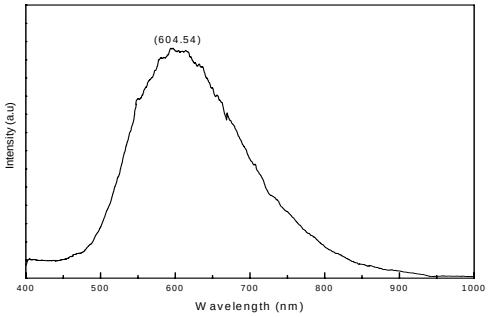

Fig. 3. Room- temperature PL spectra of the SnO_2 nanoparticles.

3.5 Raman scattering studies

Tin oxide has a tetragonal rutile crystalline structure (known in its mineral form as cassiterite) with point group D_{4h}^{14}. The unit cell consists of two metal atoms and four oxygen atoms. Each metal atom is situated amidst six oxygen atoms which approximately form the corners of a regular octahedron. Oxygen atoms are surrounded by three tin atoms which approximate the corners of the equilateral triangle. The 6 unit cell atoms give a total of 18 branches for the vibrational modes in the first Brillouin zone. The mechanical representation of normal vibration modes at the center of the Brillouin zone is given by [22]

$$\Gamma = \Gamma_1^+(A_{1g}) + \Gamma_2^+(A_{2g}) + \Gamma_3^+(B_{1g}) + \Gamma_4^+(B_{2g}) + \Gamma_5^-(E_g) + 2\Gamma_1^-(A_{2u}) + 2\Gamma_4^-(B_{1u}) + 4\Gamma_5^+(E_u),$$

Using the Koster notation with the commonly used symmetry designation listed in parenthesis. Of these 18 modes, 2 are active in infrared (the single A_{2u} and the triply degenerate E_u), 4 are Raman active (three nondegenerate modes, A_{1g}, B_{1g}, B_{2g}, and a doubly degenerate E_g), and two are silent (A_{2g}, and B_{1u}). One A_{2u} and two E_u modes are acoustic. In the Raman active modes oxygen atoms vibrate while Sn atoms are at rest (see Fig. 1 in Ref. 22). The nondegenerated modes, A_{1g}, B_{1g}, and B_{2g}, vibrate in the plane perpendicular to the c axis while the doubly degenerate E_g mode vibrate in the direction of the c axis. The B_{1g} mode consists of rotation of the oxygen atoms around the c axis, with all six oxygen atoms of the octahedra participating in the vibration. In the A_{2g} infrared active mode, Sn and oxygen atoms vibrate in the c axis direction, and in the E_u mode both Sn and O atoms vibrate in the plane perpendicular to the c axis. The silent modes correspond to vibration of Sn and O atoms in the direction of the c axis (B_{1u}) or in the plane perpendicular to this direction (A_{2g}). When size of the crystal decreases, the infrared spectrum is modified because the interaction between electromagnetic radiation and the particles depends on the crystal's size, shape and the stage of aggregation. Figure 4 shows the room temperature Raman spectra of the as grown SnO_2 nanoparticles. It can be seen that the Raman intensity is strongest for the mode A_{1g} at 633.20 cm^{-1} followed by the mode B_{2g} at 775.97 cm^{-1} and the E_g mode at 472.63 cm^{-1}; the data of A_{1g}, B_{2g} and E_g modes are in good agreement with a little shift in the peak positions compared to those observed in the previous reports [19-21, 24, 27]. Thus the Raman spectra show the typical features of the rutile phase for as prepared SnO_2 nanocrystals. However, the presence of B_{1g} mode cannot be measured in the present experiment. It is that the mode B_{1g} appears quite often with smaller nanoparticles, but is difficult to locate due to its very low intensity with respect to other modes {e.g., .001I (A_{1g})} [28] and the existence of the low frequency bands. The remarkable aspect of the Raman spectrum for as synthesized SnO_2 nanoparticles is the appearance of a new Raman peak about 501.85 cm^{-1}. This Raman peak has not been observed in the previous reports.

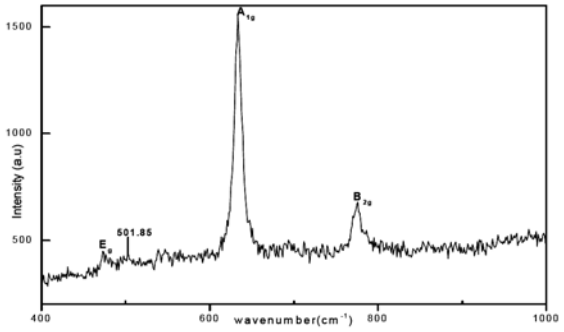

Fig. 4. Room- temperature Raman Spectrum of SnO_2 nanoparticles.

The appearance of this new mode in the nanoparticles with the particle size about to 34nm cannot be attributed to the small size of the crystals, since for the nanoparticles with this size (34nm) the wave vector is too small for bringing substantial change of the zone center photon frequency. Thus, the appearance of the additional peak cannot be attributed to the phonon confinement. In fact, the Raman active is sensitively dependent on the surface disorder – e.g., the defects and composition in the surface regions. When the grain size is small, the number of surface atoms increases greatly; for example, the surface atoms comprise 3% of the total number of atoms when the grain size is 100 nm and 30% when it is 10 nm [29]. Surface atoms are different from the inner atoms with respect to the environment of the crystal field and the binding energy and have a very large number of dangling bonds, their coordination is not completed, and they very easily combine other atoms. Besides of this, nanocrystalline SnO_2 is found in nonstochiometric form (SnO_x, x<2) [30] therefore, the large number of defects such as vacant lattice site, vacancy cluster, or local disorder at the surface and interface of nanocrystalline SnO_2, can cause the little lattice distortion and the lowering of the space symmetry, as we found a little change in the lattice parameters in our XRD studies. Change in the local symmetry of the crystal produce changes in some of the components of the polarizability tensors, even for the normally forbidden vibration modes-

i.e., due to the loss in long range order all phonons are optically possible [27]. In an intermediate case, a shift of the classical modes accompanied by broadening and the appearance of some SnO_2 forbidden modes should be observed. This is indeed what occurs with modes A_{1g}, B_{2g}, E_g, and A_{2u}. However, the new band 501.85cm^{-1} cannot fit any of the SnO_2 Raman-forbidden modes. The appearance of this new mode as a consequence of coupling between modes cannot explain the high contribution of this band observed in the spectrum of the smaller nanoparticles either. Furthermore, it is well known that the nanometer-sized crystalline materials have a crystalline component forming the crystalline nucleus and an interfacial component consisting of all the atoms situated at the grain boundaries between particles or their surfaces. The latter usually has several atomic layers in which atoms are slightly displaced from the exact position that would be suggested by the crystalline structure of the material. Thus it is possible that this new Raman peak arises from the surface layer of the nonstoichiometric SnO_x with different symmetries from SnO_2. When the grain size is small, the volume occupied by the interface and surface material increases with respect to the volume occupied by core material. It has been shown that, in the extreme case of single phase SnO_2 crystal, surface reconstruction in the (110) surface involves up to three monolayers of atoms and the presence of oxygen vacancies [31]. This gives rise to a nonstoichiometric SnO_x at the surface and this could be responsible for this new peak. It is notice that this new peak is observed in SnO_2 and not in other nanocrystalline semiconductors may be due to the high reactivity of the SnO_2 surface with environmental gases [32]. To sum up, for a nanocrystalline SnO_2 grain, a large number of vacant lattice positions and local lattice disorders can lead to change in bond length, space symmetry reduction and an obvious lattice distortion. The high Raman activity of the new vibrational mode for nanocrystals, resulting from disordered SnO_x, probably, from the interaction of surface material. In conclusion, therefore, the disorder and nanocrystalline size strongly influence the vibrational properties of this material.

4. Conclusions

Our findings indicate that the wide band gap semiconductor SnO_2 nanoparticles can be synthesized by simple and cheap hydrothermal process, offering opportunities to large-scale fabrication of other ultra fine oxide nanocrystalline materials by controlling various synthetic parameters such as; heating temperature & time, pH value of the solution, and suitable mineralizer etc. It was found that the nanocrystalline SnO_2 grains possesses structure features of the tetragonal rutile structure, but have a large amount of defects and local lattice disorder. We believe that the origin of visible emission and appearance of a new Raman peak are closely related to the presence of defects in the material, which may responsible to nonstochiometric SnO_x, lead to lowering of the space symmetry. Optical studies of nanocrystalline SnO_2 are significant for the understanding of the whole structure feature of nanomaterials and the fabrication of new nanomaterials with favorable properties.

Acknowledgements

Authors are thankful to material science group, Inter University Accelerator Center (IUAC), New Delhi for providing experimental facilities. One of the authors (Aditya Sharma) is grateful to the IUAC for providing financial support under the UFUP project (code-41304).

References

[1] O. K. Varghese, L. K.Malhotra, Sens. Actuators B, **53,** 19 (1998).
[2] D. Z.Wang, S. L.Wen, J. Chen, S. Y. Zhang, F. Q. Li, Phys. Rev. B **49**, 14282 (1994).
[3] Y. S. He, J. C. Campbell, R. C. Murphy, M. F. Arendt, J. S. Swinnea, J. Mater. Res. **8,** 3131 (1993).
[4] T. P. Hulser, H. Wiggers, F. E. Kruis, A. Lorke, Sensors and Actuators B **109,** 13 (2005).
[5] Chi-Hwan Han, Sang-Do Han, S. P. Khathar, Sensors **6,** 492 (2006).
[6] Qun Dong, Huilan Su, Di Zhang, Fangying Zhang, Nanotechnology **17,** 3968 (2006).
[7] E. Comini, G.Faglia, G. Sberveglieri, Zhengwi Pan Zhong Wang, Appl. Phys. Lett. **81,** 1869 (2002).
[8] Z. W. Pan, Z. R. Dai, Z. L. Wang, Science **291,** 1947 (2001).
[9] Z. R. Dai, Z. W. Pan, Z. L. Wang, Solid State Commun. **118,** 351 (2001).
[10] Z. R. Dai, J. L. Gole, J. D. Stout, Z. L. Wang, J. Phys. Chem. B **106**, 1274 (2002).
[11] Jr H. He, Te H. Wu, Cheng L. Hsin, Kun M. Li, Lih J. Chen, Yu L, Chueh, Li J. Chou, Zhong L. Wang, Small **2,** 116 (2006).
[12] D. P. Yu, C. S. Lee, I. Bello, X. S. Sun, Y. H. Tang, G. W. Zhou, Z. G. Bai, Z. Zhang, S. Q. Feng, Solid State Commun. **105,** 403 (1998).
[13] R. D. Tarey, T. A. Ranju, Thin Solid Films **128,** 181 (1995).
[14] F. Paraguay-Delgado, W. Antúnez-Flores, M. Miki-Yoshida, A. Aguilar-Elguezabal, P. Santiago, R Diaz, J. A. Ascencio, Nanotechnology **16,** 688 (2005).
[15] X. Zhu, R. Birringer, U. Hera, H. Gleiter, Phys. Rev B **35,** 9085 (1987).
[16] H. E. Schaefer, R. Wurschum, R. Birringer, H. Gleiter. Phys. Rev. B **38,** 9545 (1988).
[17] E. J. H. Lee, C. Ribiru, T. R. Giraldi, E. Longo, E. R. Liete, J. A. Varela, Appl. Phys. Lett. **84,** 1745 (2004).
[18] Hyoun Woo Kim, Seung Hyun Shim, Ju Hyun Myung, Brazilian J. of Phys. **35,** 1006 (2005).

[19] Soumen Das, Soumitra Kar, Subhadra Chaudhari, J. Appl. Phys. **99,** 114303 (2006).
[20] Jain Zuo, Cunyi Xu, Xianming Liu, Changsui Wang, J. Appl. Phys. **75,** 1835 (1994).
[21] K.N.Yu, Yonghong Xiong, Yulong Liu, Caoshui Xiong, Phys. Rev. B **55,** 2666 (1997).
[22] J.G.Traylor, H.G.smith, R.M.Nicklow, M. K. Wilkinson, Phys. Rev. B **3,** 3457 (1971).
[23] Francois Gervais Winfried Kress, Phys. Rev. B **31,** 4809 (1985).
[24] J. X. Zhou, M. S.Zhang, J. M. Hong, J. L. Fang, Z. Yin, Appl. Phys. A **81**, 177 (2005).
[25] L. Jiang, G. Sun, Z. Zhou, S. Sun, Q. Wang, S. Yan, H. Li, J. Tian, J. Guo, B. Zhou, Q. Xin, J. Phys. Chem. B **109** 877 (2005).
[26] G. McCarthy, J. Welton, Powder Diffr. **4,** 156 (1989).
[27] A. Dieguez, A. Romano-Rodriguez, A. Vila, J. R. Morante, J. Appl. Phys. **90,** 1550 (2001).
[28] P. S. Peercy, B. Morosin, Phys. Rev. B **7,** 2779 (1973).
[29] G. H. Wang, M. Han, Prog. Phys. **10,** 248 (1990).
[30] Z. W. Chen, J. K. Lai, C. H. Shek, Phys. Rev. B **70,** 165314 (2004).
[31] F. H. Jones, R. Dixon, J. S. Foord, R. G. Egdell, J. B. Phetica, Surf. Sci. **376,** 367 (1997).
[32] T. Pagnier, M. Boulova, A. Galerie, A. Gaskov, G. Lucazeau, J. Solid State Chem. **143,** 86 (1999).

*Corresponding author: kdverma1215868@gmail.com; kdverma12@rediffmail.com